Solar Energy Materials & Solar Cells 206 (2020) 110258

Contents lists available at ScienceDirect

Solar Energy Materials and Solar Cells

journal homepage: http://www.elsevier.com/locate/solmat

24.58% total area efficiency of screen-printed, large area industrial silicon solar cells with the tunnel oxide passivated contacts (i-TOPCon) design

Daming Chen [a,*], Yifeng Chen [a,**], Zigang Wang [a], Jian Gong [a], Chengfa Liu [a], Yang Zou [a], Yu He [a], Yao Wang [a], Ling Yuan [a], Wenjie Lin [a,b], Rui Xia [a], Li Yin [a], Xueling Zhang [a], Guanchao Xu [a], Yang Yang [a], Hui Shen [b], Zhiqiang Feng [a], Pietro P. Altermatt [a], Pierre J. Verlinden [a,b,c]

[a] State Key Lab of Photovoltaic Science and Technology, Trina Solar, ChangZhou, 213031, China
[b] Institute for Solar Energy Systems, Sun Yat-Sen University, Guangzhou, 510006, China
[c] AMROCK Pty Ltd, McLaren Vale, SA, 5171, Australia

ARTICLE INFO

Keywords:
Passivating contacts
i-TOPCon
n-type
Bifacial

ABSTRACT

We demonstrate an "industrial tunnel oxide passivated contacts" (i-TOPCon) silicon solar cell on large area n-type silicon wafers (156.75 mm × 156.75 mm). This cell has a boron diffused front emitter, a tunnel-SiO_x/n^+-poly-Si/SiN_x:H structure at the rear side, and screen-printed electrodes on both sides. The passivation of the tunnel-SiO_x/n^+-poly-Si/SiN_x:H structure on silicon wafers is investigated. The saturation currents J_o of this structure on polished and textured silicon surfaces are 1.3 and 3.7 fA/cm^2, respectively. After printing the Ag contacts, the J_o of this structure increases to 50.7 fA/cm^2 on textured silicon surfaces, which is still manageably low for metal contacts. This structure was applied to i-TOPCon solar cells, resulting in a median efficiency of 23.91%, measured in-house, and a champion efficiency of 24.58%, independently confirmed by the ISFH CalTeC in Germany. The champion efficiency was measured with total area illumination, including screen-printed fingers and busbars.

1. Introduction

In recent years, the efficiency of mainstream industrial solar cells – the passivated emitter and rear cells (PERC) – has been increased by about 0.5–0.6%$_{abs}$ per year and is presently surpassing 22% [1–3]. When approaching 23% efficiency, the majority of recombination losses will occur at the metal contacts. Hence, passivating contacts have been an intense research topic in photovoltaics for some years. Among the many different materials and structures investigated, the Tunnel Oxide Passivating Contact (TOPCon) [4] has so far attracted the interest from industry the most. In the TOPCon structure, the wafer is not contacted by metal directly. Instead, a thin tunnel oxide and then a heavily n- or p-doped poly Si layer is deposited which, finally, is contacted by metal. Because the tunnel oxide blocks one type of carrier, recombination behind the tunnel oxide does not influence device behavior, hence such structures are generally called passivating contacts. Pioneering in industry was SunPower Corporation with their interdigitated back contact (IBC) cell in 2010 [5]. Meanwhile, both laboratory world records for homo-junctions, either both-side contacted or rear-contacted, contain such passivating contacts: the n-type TopCon cell from ISE Freiburg, Germany with 25.8% efficiency [6,7], and the p-type POLO-IBC cell from ISFH, Germany, with 26.1% efficiency [8], both on 4 cm^2 designated area.

Inspired by those excellent research achievements, the attempt to introduce passivating contacts to industrial solar cell manufacturing is irresistible. Some industrial requirements need to be considered, though. Firstly, silicon wafers with large area need to be used, presently with a size of 156.75 mm × 156.75 mm or 161.7 mm × 161.7 mm. Secondly, a deposition system for poly-silicon with a high throughput is required. There are at least three different systems aiming to have mass production capability: low-pressure chemical vapor deposition (LPCVD) [9], inline plasma enhanced CVD (PECVD) [10], and inline atmospheric pressure CVD (APCVD) [11]. To the best of the authors' knowledge, the mass production verification of those deposition systems for PV industry

* Corresponding author.
** Corresponding author.
E-mail addresses: daming.chen01@trinasolar.com (D. Chen), yifeng.chen01@trinasolar.com (Y. Chen).

https://doi.org/10.1016/j.solmat.2019.110258
Received 2 September 2019; Received in revised form 24 October 2019; Accepted 25 October 2019
Available online 9 November 2019

is just at the beginning. Finally, the third important requirement is the metallization of the poly-Si thin film. Obviously, screen printing with high temperature firing is the easiest way for process integration. The difficulty is to protect the tunnel-oxide/poly-Si thin film from the destruction of the firing-through paste at high temperature. The firing-through paste removes any thin poly-Si layer and intrudes Ag nanoparticles into c-Si, increasing the saturation current J_o of the passivating contact area [12]. The saturation current density at metal contacts was reported to be 35 fA/cm^2 by Ref. [13]. Poly-Si films with thickness above 150 nm can bear the high temperature firing but these poly-Si films have a higher absorption coefficient than c-Si [14] and cause parasitic absorption losses. Therefore, developing suitable metal pastes is a challenging task for the PV industry at the moment. Despite these challenges, in the view of the levelized cost of electricity (LCOE), n-type TOPCon cells are promising candidates to become mainstream after PERC efficiency reaches about 23% [15].

We started the passivating contact research in 2015 with the purpose for mass production. We call our solar cells with passivating contacts i-TOPCon ('i' stands for 'industrial') [16]. In February 2018, our best i-TOPCon cell reached 23.03% front efficiency and 17.87% rear efficiency, accredited by JET in Japan [17]. In this report, we introduce our newly developed i-TOPCon cells from our R&D line with a maximum efficiency of 24.58%, and an open-circuit voltage of 716.8 mV, independently confirmed by ISFH CalTeC, Germany. Such cells are currently in mass production at Trina Solar, as reported elsewhere [18].

2. Experimental

2.1. Tunnel-SiO_x/n^+-poly-Si fabrication

The tunneling layer SiO_x is grown thermally in the LPCVD tube. In our industrial surroundings, we lack analytical equipment for such thin films and estimate the oxide thickness via ellipsometry on alkaline polished silicon wafers to be 1.3–1.7 nm. Controlling the tunneling thickness during the process is critical and is fine-tuned empirically.

The poly-Si layer, at least partly polycrystalline, is deposited on top of the tunnel oxide in the same LPCVD tube. Processing poly-Si thin films by LPCVD is well established in the semiconductor industry [19]. We use an industrial LPCVD system with a capacity of 1200 wafers per load. Silane is used as the gas source. The thicknesses of the as-deposited poly-Si films are measured with a scanning electronic microscope (SEM) as shown in Fig. 1. In one experiment, the deposition time was varied to obtain several thicknesses of poly-Si films. From correlating thickness with deposition time in Fig. 1(c), we obtained a deposition rate on polished and textured silicon wafers of about 3.3 nm/min and about 3.1 nm/min.

The as-deposited intrinsic poly-Si is subsequently doped with a $POCl_3$ diffusion to form n^+-poly-Si, which is necessary so tunneled electrons find a state in the conduction band, and also to pin the Fermi level in the poly-layer so electrons become accumulated in front of the tunneling layer and – last but not least – to reduce SRH recombination at the wafer/oxide interface. To investigate the surface passivation effect of this structure on silicon wafers, symmetrical samples on 5 Ωcm n-type Cz silicon wafers were fabricated for measuring the effective lifetime and J_o. To study the influence of surface morphology on the passivation, one group of the samples was polished in a 10% KOH solution at 80 °C for 3 min, the other group was pyramid textured in a 2% KOH solution containing an additive at 70 °C for 6 min. After polishing or texturization, the samples were cleaned with a standard RCA cleaning procedure. Then the tunnel oxide was grown on both sides, followed by the intrinsic poly-Si deposition. The thicknesses of intrinsic poly-Si on polished and textured surface were estimated to be 297 nm and 279 nm respectively based on the deposition rate described in previous paragraph. Then the intrinsic poly-Si was doped with a $POCl_3$ diffusion followed by an RCA cleaning. To supply enough hydrogen for passivation, SiN_x:H thin films were added on both sides by PECVD. Finally, the samples were fired with

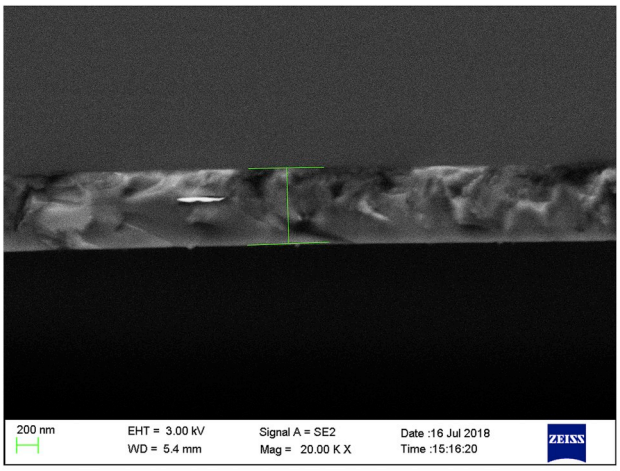

(a)

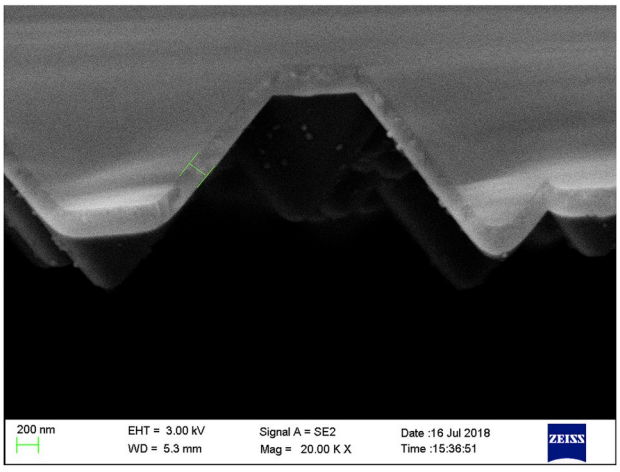

(b)

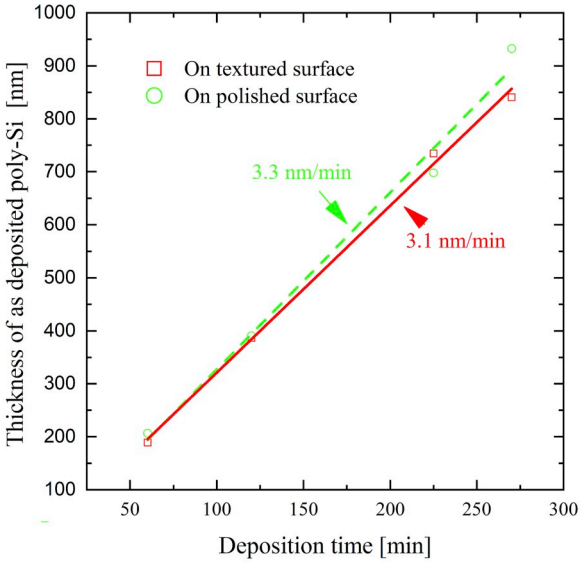

(c)

Fig. 1. SEM pictures of SiO_x/n^+-poly-Si stacks on (a) alkaline polished Si wafers and (b) textured wafers,and (c) the thickness of poly-Si measured by SEM as a function of deposition time.

an industrial belt firing furnace with a peak temperature of ~760 °C. The effective excess carrier lifetime was measured with a Sinton WCT-120 set-up in quasi-steady mode, and the surface J_o values were extracted with the method of Kane and Swanson [20] applying procedures described in Ref. [21] and using in the data evaluation the intrinsic carrier density of 8.6×10^9 cm^{-3} (the value at 25 °C).

The passivation ability of the tunnel-SiO_x/n^+-poly-Si/SiN_x:H stack after metallization was also investigated. The same type of samples with pyramid textured surfaces as in the above J_o measurement were screen printed with Ag contact lines at one side only, having 9 different pitches. Then the Ag paste was fired through the nitride in an industrial belt firing furnace with the finger-side facing down, at the peak firing temperature of 760 °C. Afterwards, the fingers were etched off with aqua-regia solution (V_{HCl} : V_{HNO_3} = 3:1). Finally, the samples were rinsed in DI water and spin dried. Photoluminescence images of the samples were taken with a BTi-LIS-R1 from BT Imaging, and the J_o values for the 9 respective metallization fractions f were extracted with the same Sinton WCT-120 tool as the above J_0 measurements.

2.2. i-TOPCon solar cell fabrication

The stacks were integrated into n-type bifacial solar cells, named i-TOPCon solar cells. The cell structure is illustrated in Fig. 2. It features a front boron emitter and a rear passivating contact, with screen-printed fingers on both sides to obtain bifaciality. The phosphorus-doped wafers contain only low amounts of oxygen, with a resistivity range of about 0.5 Ωcm to 1 Ωcm. The cell fabrication sequence is indicated in Fig. 3. The wafers are double-side textured with random pyramids in a KOH solution. After RCA cleaning, the boron emitter is formed in a boron diffusion furnace using a BBr_3 source. The rear boron diffusion is removed by a single side etching process using HF/HNO_3. After chemical cleaning, a tunneling SiO_x is thermally grown and an intrinsic poly-Si film (at least partly polycrystalline) is deposited in a LPCVD system. The intrinsic poly-Si is doped in a $POCl_3$ diffusion furnace subsequently to convert to n^+-poly-Si. Another single side etching process is applied to remove the front side wrap-around poly-Si. After another RCA cleaning, the boron emitter is passivated with dielectric films, which also acts as an anti-reflective coating stack. The rear side SiO_x/n^+-poly-Si stack is coated with PECVD SiN_x:H. For metallization, an "H- metal-contact" pattern with 9 busbars is screen printed on both sides, followed by a fast firing process with a peak temperature of about 760 °C. After fabrication, the IV curve and other valuable parameters are measured with a Sinton FCT-450 flasher.

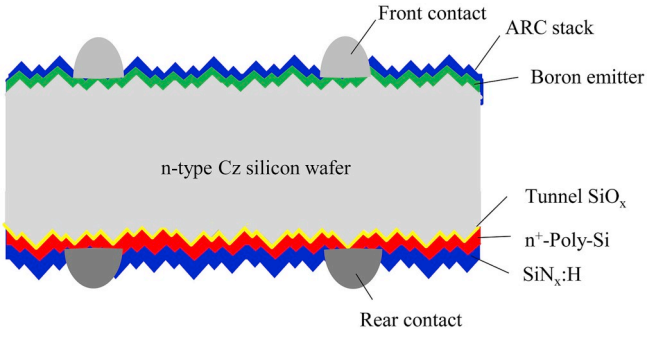

Fig. 2. Schematic of i-TOPCon solar cells on n-type monocrystalline silicon wafers. (For interpretation of the references to colour in this figure legend, the reader is referred to the Web version of this article.)

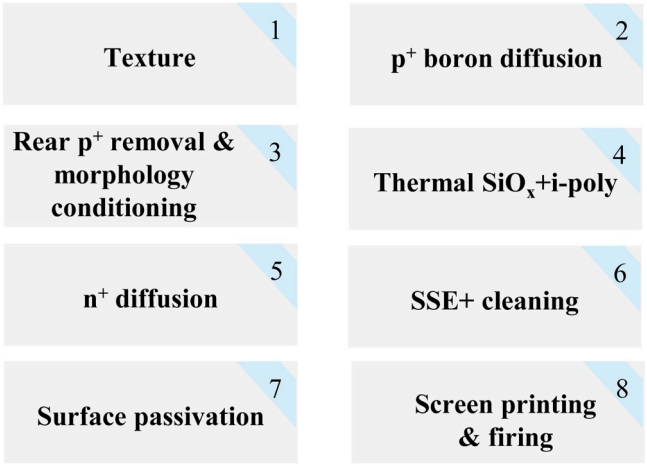

Fig. 3. Process flow of i-TOPCon solar cells.

3. Results and discussions

3.1. Passivation properties of the tunnel-SiO_x/n^+-poly-Si/SiN_x:H structure

The poly-Si thin films were "ex-situ" doped with $POCl_3$ diffusion in a standard furnace. By optimizing the diffusion process, excellent surface passivation was achieved on both polished and textured surfaces. Fig. 4 shows the injection dependent saturation current J_o, which for polished and textured surface are 1.3 and 3.7 fA/cm^2, respectively, at their maximum at the excess carrier density of 3×10^{15} cm^{-3} [21]. The results are close to previous literature values [9], where the poly-Si films were also deposited by LPCVD.

For the passivating contact, firing-through Ag paste was used for metallization. As the paste may deteriorate the passivation ability of the

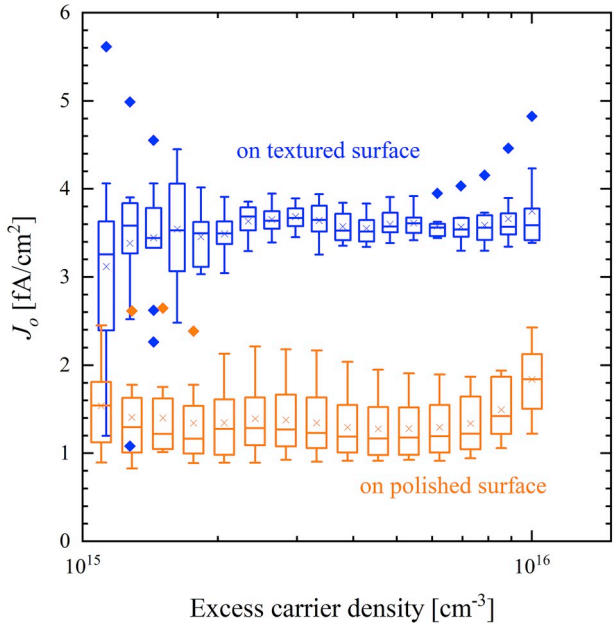

Fig. 4. Saturation current density J_0 of the SiO_x/n^+-poly-Si/SiN_x:H stack on textured (blue) or alkaline polished (orange) n-type silicon wafers. For the extraction of J_0 from the effective excess carrier lifetime data, the intrinsic carrier density of $n_i = 8.6 \times 10^9$ cm^{-3} is used (value for 25 °C). The line in the boxes is the median value, the cross the average value. Outsiders are marked as symbols. (For interpretation of the references to colour in this figure legend, the reader is referred to the Web version of this article.)

stack, we screen-printed samples with 9 different metallization fractions as described in Section 2.1. Fig. 5 shows the photoluminescence (PL) of a sample after firing and removing the Ag contact lines. The J_0 of the metallization regions, $J_{0,cont,}$ was extracted from the local J_0 measurements using the formula:

$$J_{0,tot} = J_{0,pass,front} + (1-f)J_{0,pass,rear} + fJ_{0,cont} = (J_{0,cont} - J_{0,pass})f + 2J_{0,pass} \quad (1)$$

The total saturation current, $J_{0,tot}$, is the sum of the passivated front side ($J_{0,pass,\ front}$) and the rear side, which had metallization fraction f and therefore is taken as the sum of contacted and passivated parts. The second line of equation (1) assumes that the passivation of the uncontacted parts has the same quality at the front and at rear side. Fig. 6 shows $J_{0,tot}$ vs. f. From equation (1), the slope of $J_{0,tot}$ vs. f is equal to $J_{0,cont}$ - $J_{0,pass}$, and the intercept with the y-axis is equal to $2J_{0,pass}$. In Fig. 6, the resulting $J_{0,cont}$ is 50.7 fA/cm^2, and the resulting $J_{0,pass}$ is 4.4 fA/cm^2. Indeed, the Ag paste degrades the passivation effect of the stack. Further improvement may come from developing a better suitable Ag paste for poly-Si, or from using alternative metallization methods such as evaporation. The rear side metallization of our bifacial solar cells is around 6%, therefore the total J_o at the rear side of the cells is estimated to be 7 fA/cm^2.

The above analysis shows that the passivating contact has an excellent passivation performance. Furthermore, for device application, the electron transport must be successful in order to maintain a low series resistance of the solar cell. The research of electron transport through thin SiO_x is beyond the scope of this work. There exist two different models for the carrier transporting across the SiO_x interface, the tunneling model [22] and the pinholes model [23]. Nevertheless, both show low contact resistivities of the SiO_x/n + -poly-Si structure [22–24].

3.2. Application of the tunnel-SiO_x/n$^+$-poly-Si/SiN_x:H structure on i-TOPCon solar cells

In a small experiment, two groups of i-TOPCon solar cells with the rear side SiO_x/n$^+$-poly-Si/SiN_x:H structure were fabricated: one is the baseline, the other is with an improved process to enhance the infrared spectral response.

The IV parameters were measured with the Sinton FCT-450 flash tester as listed in Table 1, however without precise reference cells available and with home-made probe bars at that time. Hence, the short circuit current J_{sc} and fill factor FF may be inaccurate. The median cell efficiency of the baseline group is 23.86%, with a maximum efficiency of 24.09%. And the median efficiency of the improved group is 23.91%,

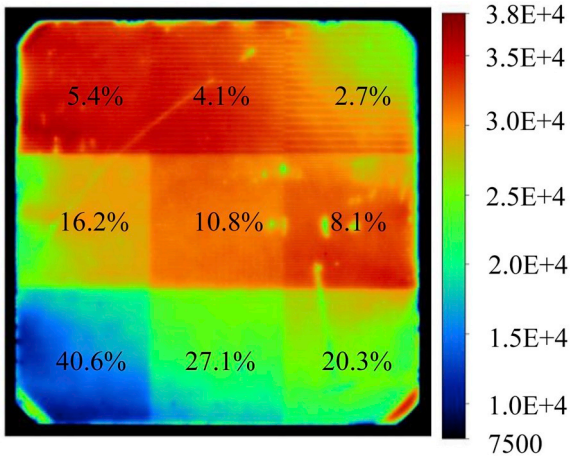

Fig. 5. Photoluminescence (PL) images (counts) of symmetric SiO_x/n$^+$-poly-Si/SiN_x:H passivated samples with 9 different metallization fractions one the rear side. The metal was etched away before the PL measurement. The numbers in percentage indicate the metallization fractions.

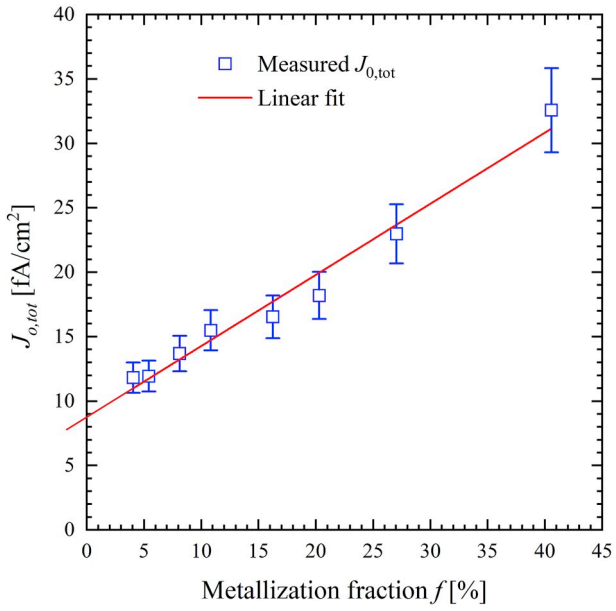

Fig. 6. Measured total J_0 vs. the metallization fraction f of the symmetrically SiO_x/n$^+$-poly-Si/SiN_x:H passivated samples for the extraction of J_0 at the contact regions.

Table 1
In-house measured IV parameters of i-TOPCon solar cells in a small experiment.

	Cell quantity		J_{sc} [mA/cm^2]	V_{oc} [V]	FF [%]	η [%]
Baseline	14	Median	40.57	0.712	82.56	23.86
		Maximum	40.63	0.714	83.12	24.09
Improved	9	Median	40.80	0.712	82.23	23.91
		Maximum	40.89	0.716	82.85	24.14

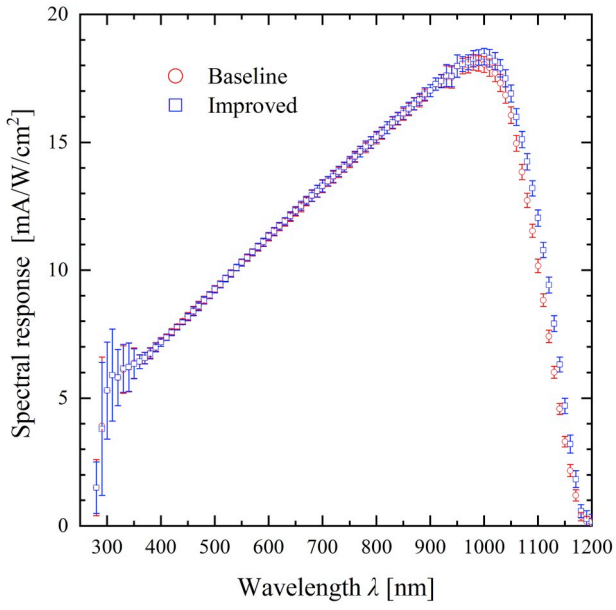

Fig. 7. Spectral response of the i-TOPCon solar cells from the baseline process (red) and the improved process (blue), as measured by ISFH CalTeC. (For interpretation of the references to colour in this figure legend, the reader is referred to the Web version of this article.)

with a maximum efficiency of 24.14%. J_{sc} of cells from the improved group are 0.2–0.3 mA/cm^2 higher than in the baseline group. From spectral response measurements made later at the ISFH CalTeC, shown in Fig. 7, we conclude that the gain in J_{sc} is due to the better spectral response at long wavelength between 1000 and 1200 nm, which depends on the deposition conditions of the poly-Si layer.

The Sinton FCT-450 flash tester also measures the effective lifetime τ_{eff}, shown in Fig. 8(a), from the decay of illumination level and V_{oc} and using the procedures described in Ref. [25]. At the maximum power point (V_{mpp}) condition, τ_{eff} is about 900 µs, however is significantly lower at the open-circuit (V_{oc}) condition due to thermal donors. Therefore, the cell's total J_o is larger near V_{oc} than near V_{mpp}, causing an increase of *FF* as discussed in Ref. [26]. Hence, thermal donors do not increase the efficiency, they decrease V_{oc} and hence increase *FF*. We do not know the reason why τ_{eff} decreases at low injection densities so strongly. The sum of J_0 of the front side and the rear side of solar cells are extracted from the inverse τ_{eff} with Auger correction, as shown in Fig. 8(b): a low J_0 down to 25 fA/cm^2 is reached. The total lumped R_s is measured by comparing the sun-V_{oc} curve with the IV points measured at 1-sun and is 0.320 Ωcm^2.

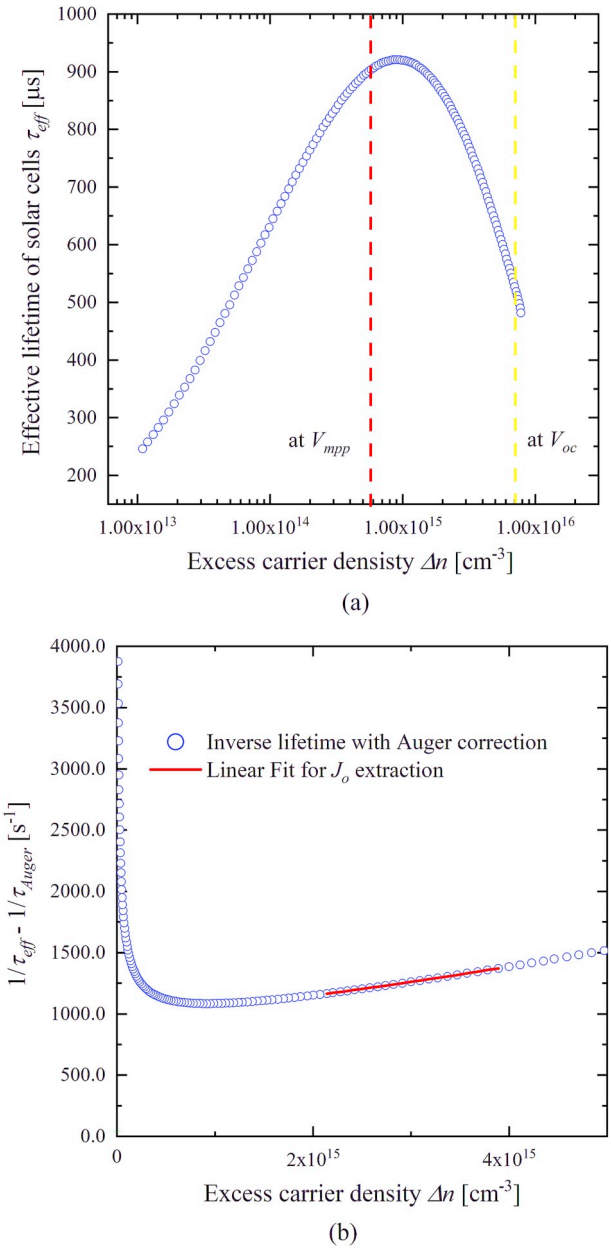

Fig. 8. Effective lifetime τ_{eff} of an i-TOPCon cell measured by Suns-V_{oc} with the Sinton FCT-450 flash tester (a), and the inverse effective lifetime with Auger correction for J_o extraction (b).

The Sinton FCT-450 software performs also an automatic power loss analysis. The recombination losses in the diffused regions and in the base region, respectively, are given in percent of J_{sc}:

$$\frac{\frac{J_0\left(\Delta n+N_{dop}\right)\Delta n}{n_i^2}}{J_{sc}} \times 100 \tag{2}$$

$$\frac{\frac{qW\Delta n}{\tau_{bulk}}}{J_{sc}} \times 100 \tag{3}$$

while the resistive losses are given in percentage of voltage loss to the maximum power voltage if there were no series resistance, the R_s-free $pV_{\mathrm{mpp}} = V_{mpp} + J_{mpp}R_s$:

$$\frac{J_{mpp}R_s}{V_{mpp}+J_{mpp}R_s} \times 100 \tag{4}$$

Fig. 9 shows the results. The dominating loss is from recombination at the front side and rear side of the cells. Since the rear side is well passivated by the passivating contact, we know that the major loss comes from the boron-diffused front side emitter. Improving the emitter and its metallization still bears a large potential for further efficiency improvements.

Several solar cells were sent to ISFH CalTeC for third-party certification. Particularly 9 contact bars were used for contacting the front 9 busbars of solar cells, and a brass copper chunk which with high reflection and high conduction was used to contact the other side of solar cells. The best bifacial solar cell reached a front side efficiency of 24.58%, and a rear side efficiency of 19.48%, on its full 244.62 cm^2 wafer area including metal fingers and bus bars, without using any dedicated aperture during the illumination. The IV curves and IV parameters of this champion solar cell are shown in Fig. 10. The fill factor is high due to thermal donors [26], as outlined above. The bifaciality is 79.25% according to the difference of efficiency under front side illumination and under rear side illumination.

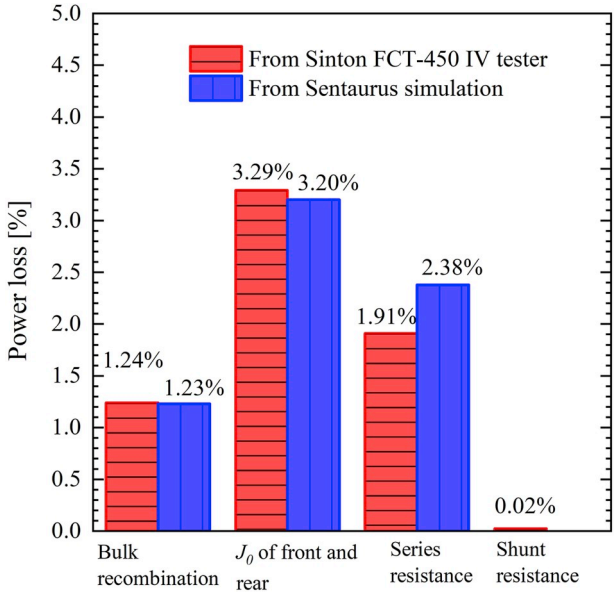

Fig. 9. Power loss of i-TOPCon solar cells due to different loss channels, measured with the Sinton FCT-450 flash tester (red columns) compared to Sentaurus simulations in Chap. 4 (blue columns). (For interpretation of the references to colour in this figure legend, the reader is referred to the Web version of this article.)

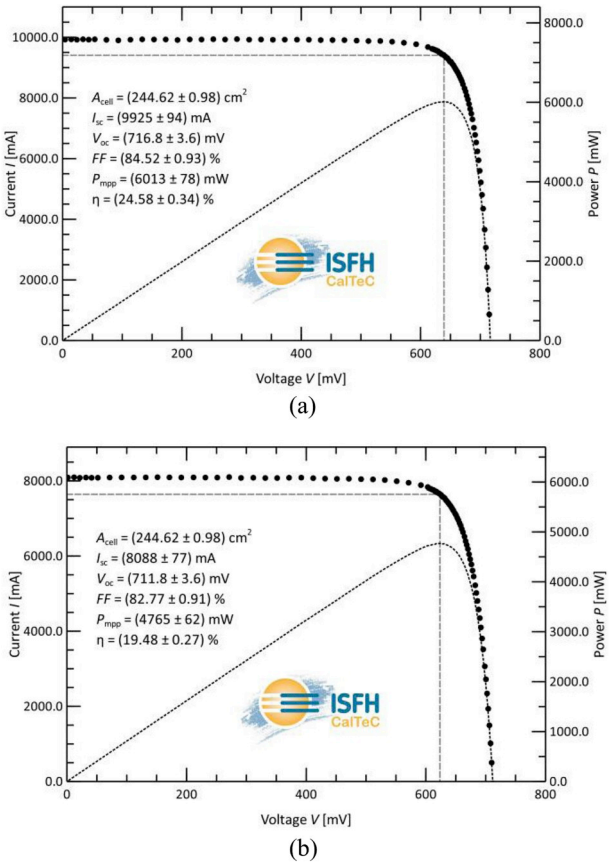

Fig. 10. IV curves and parameters of the champion i-TOPCon solar cell measured at ISFH CalTeC, (a) under front side illumination, (b) under rear side illumination.

4. Modeling

Numerical device modeling with Sentaurus [27] is used for a detailed loss analysis. The silicon parameters are taken from Ref. [28] with an update from Ref. [29] for Auger recombination, leaving the small material uncertainties given in Ref. [30].

The J_0 measurements were reproduced with simulations using measured ECV dopant profiles as input, where the surface recombination velocity S is extracted as the only free parameter to assess the passivation quality. Somewhat surprisingly, S of the tunnel oxide is not lower than reported in literature [31,32] about oxides at the surface where no poly-Si was used, implying that the n^+-poly-Si layer does not improve oxide passivation. In our understanding, outlined in Ref. [33], this makes sense: SiO_2 is passivated mainly by the H^+ species because the dominating P_L dangling bonds are donor-like (the amphoteric U_M states do not contribute to recombination as much). The H^+ species is abundant in both configurations [34]: when (i) the n-type wafer is passivated by both SiO_2 and n^+-poly-Si or (ii) by SiO_2 only. In contrast, p + -poly-Si layers improve SiO_2 passivation significantly compared to solely SiO_2 on boron-diffused surfaces because the p + -poly-Si provides an abundance of H^+. Our finding implies for the n + -poly-Si passivating contacts in general that the low J_0 values are mainly achieved by optimizing the phosphorus dopant profile caused by diffusion of phosphorus from the n^+-poly-Si layer through the tunnel oxide into the Si wafer. Basically, the poly layer is a limited phosphorus source and the tunnel oxide acts as a welcome limitation to phosphorus diffusion but is not passivated better than oxides at the surface. In our case, the n^+-poly-Si layer is doped about 1.5×10^{20} cm^{-3}, but the peak doping concentration at the oxide is near 10^{19} cm^{-3}, and the diffusion reaches about 80 nm deep into the wafer. Our device simulations in Fig. 11 show that there is

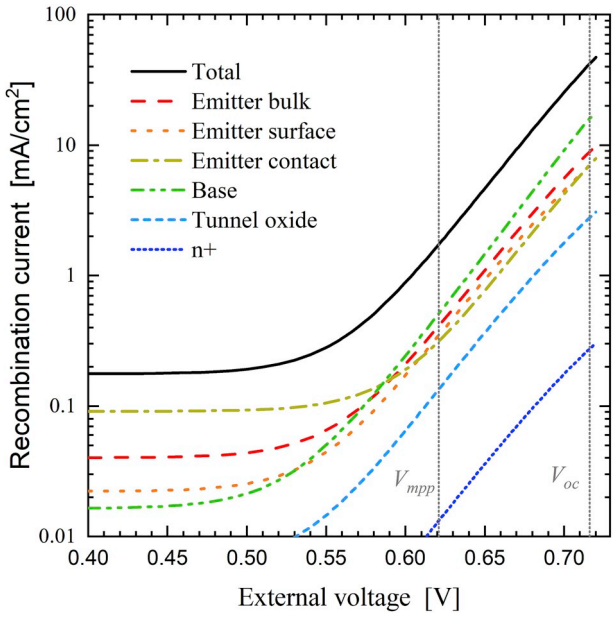

Fig. 11. Simulated recombination losses of the indicated device regions.

about ten times more recombination at the tunnel oxide than there is in the bulk of the diffusion (the 80 nm deep wafer region below the SiO_x layer), thus the passivation quality of the tunnel oxide plays a significant role.

To assess the amount of recombination losses in the various device regions, we integrate the recombination rates over these regions and plot them in Fig. 11. Although these losses are simulated locally with the local split of the quasi-Fermi energy levels, the losses are plotted with the external voltage V_{ext} because it is V_{ext} that matters for device efficiency.

Fig. 11 indicates that the cell is well optimized because the main recombination losses have similar magnitude at mpp: in the base region (dominated by Auger), in the bulk of the emitter, at its surface, and at its metal contacts. The losses at the rear passivating contact are far smaller despite the screen-printing assessed in the previous chapter. Crucial (and most uncertain in the simulations) are the recombination losses at the emitter contacts; they can easily dominate the losses at the front if the chosen screen-printing paste and the firing conditions are not as optimized. The simulated total lumped R_s is 0.389 Ωcm^2, which is higher than 0.320 Ωcm [2] measured with the Sinton tester.

The comparison of the simulated losses with the measured losses is shown in Fig. 9. The simulated recombination in the base is 0.5 mA/cm^2, hence 0.5/40.57 = 1.23% of J_{sc} as measured with the Sinton tester; the simulated recombination in the diffused regions is 1.3/40.54 = 3.20% compared to the measured 3.29%. While the recombination losses agree well, the simulated resistive losses are higher: simulated is $0.389 \times 39.0/(622 + 0.389 \times 39.0) = 2.38\%$ of V_{mpp}, compared to the measured 2.0%. This may be due to the strong injection-dependence of τ_{eff} near and below mpp, which may not be caused by homogeneous recombination but by other effects.

A ray tracing analysis with SunSolve from PV Lighthouse [35] reveals that the optical losses are dominated by escape at long wavelengths followed by front reflectivity, followed by parasitic absorption losses in the poly-Si, which are only 0.035 to 0.06 mA/cm^2 depending on the deposition conditions of the poly-Si [36].

5. Conclusions

In our development of i-TOPCon cells, it was instrumental to use a series of test samples and elaborated analysis for reaching an independently confirmed champion efficiency of 24.58%. The reported

efficiency is on large wafer including metal fingers and bus bars, full illumination, and fabricated with industrial equipment (no photolithography etc.). The analysis shows that recombination losses in the emitter, including its bulk, surface and metal contacts are limiting the device performance, while the rear passivating contact has a low J_0 of less than 7 fA/cm^2, including the 94% non-metallized region with $J_0 = 3.4$ fA/cm^2 as well as 6% metallization area with $J_0 = 50.7$ fA/cm^2. We conclude that improving the emitter and its metallization still bears a large potential for further efficiency improvements. This may be done with further development of a conventional emitter structure and its metallization paste, or with replacing it by a transparent passivating contact. In our opinion, simplifying the process flow of poly-Si passivating contacts, as well as developing a transparent passivating contact that is industrially feasible, are presently one of the most urgent tasks in Si photovoltaic research and development.

Declaration of competing interest

The authors declare that they have no known competing financial interests or personal relationships that could have appeared to influence the work reported in this paper.

Acknowledgements

This work is supported by the National Key R&D Program of China [grant number 2018YFB1500503].

Appendix A. Supplementary data

Supplementary data to this article can be found online at https://doi.org/10.1016/j.solmat.2019.110258.

References

[1] M. Hermle, Silicon Solar Cells – Current Production and Future Concepts, Annual Conference of the European Technology and Innovation Platform Photovoltaics - "PV Manufacturing in Europe", May 2017, pp. 18–19.
[2] F. Stenzel, B.G. Lee, J. Cieslak, A. Schwabedissen, D. Wissen, S. Geißler, T. Rudolph, B. Faulwetter-Quandt, R. Hönig, S. Wasmer, R. Bakowskie, D. Buß, F. Fertig, M. Schaper, A. Mette, J.W. Müller, Exceeding 23% and mass production of p-Cz Q.ANTUM bifacial solar cells, in: Proceedings of the 36th European Photovoltaic Solar Energy Conference and Exhibition, Marseille, France, 2019, pp. 96–99.
[3] Aiko solar news release. http://en.aikosolar.com/news_detail/newsId=37.html.
[4] F. Feldmann, M. Bivour, C. Reichel, M. Hermle, S.W. Glunz, Passivated rear contacts for high-efficiency n-type Si solar cells providing high interface passivation quality and excellent transport characteristics, Sol. Energy Mater. Sol. Cells 120 (2014) 270–274, https://doi.org/10.1016/j.solmat.2013.09.017.
[5] P.J. Cousins, D.D. Smith, H. Luan, J. Manning, T.D. Dennis, A. Waldhauer, K. E. Wilson, G. Harley, W.P. Mulligan, Generation 3: improved performance at lower cost, in: Proceedings of the 35th IEEE Photovoltaic Specialists Conference, Honolulu, HI, USA, 20-25 June 2010, pp. 00275–00278.
[6] A. Richter, J. Benick, F. Feldmann, A. Fell, M. Hermle, S.W. Glunz, N-Type Si solar cells with passivating electron contact: identifying sources for efficiency limitations by wafer thickness and resistivity variation, Sol. Energy Mater. Sol. Cells 173 (2017) 96–105, https://doi.org/10.1016/j.solmat.2017.05.042.
[7] M.A. Green, Y. Hishikawa, E.D. Dunlop, D.H. Levi, J. Hohl-Ebinger, A.W.Y. Ho-Baillie, Solar cell efficiency tables (version 51), Prog. Photovolt.: Res. Appl. 26 (1) (2018) 3–12, https://doi.org/10.1002/pip.2978.
[8] F. Haase, C. Hollemann, S. Schäfer, A. Merkle, M. Rienäcker, J. Krügener, R. Brendel, R. Peibst, Laser contact openings for local poly-Si-metal contacts enabling 26.1%-efficient POLO-IBC solar cells, Sol. Energy Mater. Sol. Cells 186 (2018) 184–193, https://doi.org/10.1016/j.solmat.2018.06.020.
[9] M.K. Stodolny, M. Lenes, Y. Wu, G.J.M. Janssen, I.G. Romijn, J.R.M. Luchies, L. J. Geerligs, n-Type polysilicon passivating contact for industrial bifacial n-type solar cells, Sol. Energy Mater. Sol. Cells 158 (1) (2016) 24–28, https://doi.org/10.1016/j.solmat.2016.06.034.
[10] N. Nandakumar, J. Rodriguez, T. Kluge, T. Groβe, L. Fondop, P. Padhamnath, N. Balaji, M. König, S. Duttagupta, Approaching 23% with large-area monoPoly cells using screen-printed and fired rear passivating contacts fabricated by inline PECVD, Prog. Photovolt.: Res. Appl. 27 (2) (2018) 107–112, https://doi.org/10.1002/pip.3097.
[11] A. Merkle, S. Seren, H. Knauss, B. Min, J. Steffens, B. Terheiden, R. Brendel, R. Peibst, Atmospheric pressure chemical vapor deposition of in-situ doped amorphous silicon layers for passivating contacts, in: Proceedings of the 35th European Photovoltaic Solar Energy Conference and Exhibition, 2018, pp. 785–791.
[12] M.K. Stodolny, J. Anker, B.L.J. Geerligs, G.J.M. Janssen, B.W.H. van de Loo, J. Melskens, R. Santbergen, O. Isabella, J. Schmitz, M. Lenes, J. Luchies, W.M. M. Kessels, I. Romijn,Material properties of LPCVD processed n-type polysilicon passivating contacts and its application in PERPoly industrial bifacial solar cells, Energy Procedia 124 (2017) 635–642, https://doi.org/10.1016/j.egypro.2017.09.250.
[13] P. Padhamnath, J. Wong, B. Nagarajan, J.K. Buatis, L.M. Ortega, Naomi Nandakumar, A. Khanna, V. Shanmugam, S. Duttagupta, Metal contact recombination in monoPoly™ solar cells with screen-printed & fire-through contacts, Sol. Energy Mater. Sol. Cells 192 (2019) 109–116, https://doi.org/10.1016/j.solmat.2018.12.026.
[14] F. Feldmann, C. Reichel, R. Müller, M. Hermle, The application of poly-Si/SiOx contacts as passivated top/rear contacts in Si solar cells, Sol. Energy Mater. Sol. Cells 159 (2017) 265–271, https://doi.org/10.1016/j.solmat.2016.09.015.
[15] P.J. Verlinden, Prospect of Manufacturing of High-Efficiency Photovoltaics for a Transformed Sustainable Energy Economy, Presentation in PV CellTech 2018, Penang, Malaysia, March 2018.
[16] Y. Chen, D. Chen, P.P. Altermatt, G. Xu, Z. Wang, C. Liu, Y. Zou, Y. He, Y. Wang, J. Gong, L. Yuan, W. Liu, Y. Chen, M. Deng, Y. Hu, S. Chen, J. Xiang, H. Shen, S. Zhang, L. Wang, X. Zhang, Y. Yang, Z. Feng, P.J. Verlinden, Toward 25% silicon cell efficiency in mass-production: strategies and prospects based on industrial data, in: Proceedings of the 36th European Photovoltaic Solar Energy Conference and Exhibition, Marseille, France, 2019, pp. 298–303.
[17] Y. Chen, D. Chen, C. Liu, Z. Wang, Z. Yang, Y. He, G. Xu, X. Zhang, Y. Yang, P. P Altermatt, Z. Feng, P. Verlinden, The path to 25% large-area industrial crystalline silicon solar cells, in: 3rd N-type C-Si Cell and Passivated Contact Forum, Changzhou, 2018.
[18] Y. Chen, D. Chen, C. Liu, Z. Wang, Y. Zou, Y. He, Y. Yao, L. Yuan, J. Gong, W. Lin, X. Zhang, Y. Yang, H. Shen, Z. Feng, P.P. Altermatt, P.J. Verlinden, Mass production of industrial tunnel oxide passivated contacts (i-TOPCon) silicon solar cells with average efficiency over 23% and modules over 345 W, Prog. Photovolt.: Res. Appl. 27 (10) (2019) 827–834, https://doi.org/10.1002/pip.3180.
[19] A.R. Coulson, R.N. Tauber, Amorphous and polycrystalline thin films, in: S. Wolf, R.N. Tauber (Eds.), Silicon Processing for the VLSI Era, Volume 1: Process Technology, Lattice Press, USA, 1986, pp. 161–195 (chapter 6).
[20] D.E. Kane, R.M. Swanson, Measurement of the emitter saturation current by a contactless photoconductivity delay method, in: Proceedings of the 18th IEEE Specialist Conference, Las Vegas, 1985, pp. 578–583.
[21] B. Liu, Y. Chen, Y. Yang, D. Chen, Z. Feng, P.P. Altermatt, P. Verlinden, H. Shen, Improved evaluation of saturation currents and bulk lifetime in industrial Si solar cells by the quasi steady state photo conductance decay method, Sol. Energy Mater. Sol. Cells 149 (2016) 258–265, https://doi.org/10.1016/j.solmat.2016.01.032.
[22] F. Feldmann, G. Nogay, J. Polzin, B. Steinhauser, A. Richter, A. Fell, C. Schmiga, M. Hermle, S.W. Glunz, A study on the charge carrier transport of passivating contacts, IEEE J. Photovoltaics. 8 (2018) 1503–1509, https://doi.org/10.1109/JPHOTOV.2018.2870735.
[23] R. Peibst, U. Römer, Y. Larionova, M. Rienäcker, A. Merkle, N. Folchert, S. Reiter, M. Turcu, B. Min, J. Krügener, D. Tetzlaff, E. Bugiel, T. Wietler, R. Brendel, Working principle of carrier selective poly-Si/c-Si junctions: Is tunnelling the whole story? Sol. Energy Mater. Sol. Cells 158 (2016) 60–67, https://doi.org/10.1016/j.solmat.2016.05.045.
[24] G. Kökbudak, R. Müller, F. Feldmann, A. Fell1, R. Turan, S.W. Glunz, On the determination of the contact resistivity for passivating contacts using 3D simulations, in: Proceedings of the 33rd European Photovoltaic Solar Energy Conference and Exhibition, 2017, pp. 242–246.
[25] M.J. Kerr, A. Cuevas, R.A. Sinton, Generalized analysis of quasi-steady-state and transient decay open circuit voltage measurements, J. Appl. Phys. 91 (2002) 399, https://doi.org/10.1063/1.1416134.
[26] W. Duan, S. Yuan, Y. Sheng, W. Cai, Y. Chen, Y. Yang, P.P. Altermatt, Z. Feng, P. J. Verlinden, A route towards high efficiency N-type PERT solar cells, in: Proceedings of the 32nd European Photovoltaic Solar Energy Conference and Exhibition, Munich, Germany, 2016, pp. 399–402.
[27] Sentaurus Device User Guide, Synopsys Inc., Mountain View, CA.
[28] P.P. Altermatt, Models for numerical device simulations of crystalline silicon solar cells - a review, J. Comput. Electron. 10 (2011) 314–331, https://doi.org/10.1007/s10825-011-0367-6.
[29] B.A. Veith-Wolf, S. Schäfer, R. Brendel, J. Schmidt, Reassessment of intrinsic lifetime limit in n-type crystalline silicon and implication on maximum solar cell efficiency, Sol. Energy Mater. Sol. Cells 186 (2018) 194–199, https://doi.org/10.1016/j.solmat.2018.06.029.
[30] S. Wasmer, A. Fell, J.M. Greulich, Influence of fundamental model uncertainties on silicon solar cell efficiency simulations, IEEE Trans. Electron Devices 66 (2019) 524–532, https://doi.org/10.1109/ted.2018.2882776.

[31] A. Kimmerle, M.M. Rahman, S. Werner, S. Mack, A. Wolf, A. Richter, H. Haug, Precise parameterization of the recombination velocity at passivated phosphorus doped surfaces, J. Appl. Phys. 119 (2016) 25706, https://doi.org/10.1063/1.4939960.
[32] P.P. Altermatt, J.O. Schumacher, A. Cuevas, M.J. Kerr, S.W. Glunz, R.R. King, G. Heiser, A. Schenk, Numerical modeling of highly doped Si:P emitters based of Fermi-Dirac statistics and self-consistent material parameters, J. Appl. Phys. 92 (2002) 3187–3197, https://doi.org/10.1063/1.1501743.
[33] Y. Yang, P.P. Altermatt, Y. Cui, Y. Hu, D. Chen, L. Chen, G. Xu, X. Zhang, Y. Chen, P. Hamer, R.S. Bonilla, Z. Feng, P.J. Verlinden, Effect of carrier-induced hydrogenation on the passivation of the poly-Si/SiOx/c-Si interface, AIP Conf. Proc. 1999 (2018) 40026, https://doi.org/10.1063/1.5049289.
[34] C. Sun, F.E. Rougieux, D. Macdonald, A unified approach to modelling the charge state of monatomic hydrogen and other defects in crystalline silicon, J. Appl. Phys. 117 (2015) 45702, https://doi.org/10.1063/1.4906465.
[35] P.V. Lighthouse, Coledale, NSW, Australia. https://www.pvlighthouse.com.au/.
[36] B. Min, M.R. Vogt, T. Wietler, R. Reineke-Koch, B. Wolpensinger, E. Köhnen, D. Tetzlaff, C. Schinke, R. Brendel, R. Peibst, Increasing the photo-generated current in solar cells with passivating contacts by reducing the poly-Si deposition temperature, AIP Conf. Proc. 1999 (2018) 40015, https://doi.org/10.1063/1.5049278.